J Mol Model (2011) 17:2227–2235
DOI 10.1007/s00894-010-0887-1

ORIGINAL PAPER

Molecular dynamics of the "hydrophobic patch" that immobilizes hydrophobin protein HFBII on silicon

Clara Moldovan · Damien Thompson

Received: 14 September 2010 / Accepted: 20 October 2010 / Published online: 9 November 2010

Abstract The experimentally-observed stable, electrically-conducting interface formed between hydrophobin protein HFBII and silicon provides a model system for the Bio/ICT interfaces required for bionanoelectronics. The present work used molecular dynamics (MD) computer simulations to investigate the atom-scale details of the assembly and structure of the HFBII/silicon interface, using models on the order of 40,000 atoms to compute energy profiles for the full protein interacting with a bare Si(111) substrate in aqueous solution. Five nanoseconds of free, equilibrated dynamics were performed for six models with initial protein:silicon separations ranging from 1.2 to 0.2 nanometers in steps of 0.2 nm. Three of the models formed extensive protein:silicon van der Waals's interfacial contacts. The model with 0.2 nm starting separation serves as an illustrative example of the dynamic interface created, whereby hydrophobic patch residues cycle between flat and more protruding patch conformations that favor respectively close inter-patch and close patch-surface contacts, with protein:surface separations cycling between 0.2 and 0.4 nm over the 5 ns of dynamics. Analysis of residue-based binding energies at the interface reveal three leucines Leu19, Leu21 and Leu63, together with isoleucine Ile22 and alanine Ala61, as the primary drivers towards adhesion on bare silicon, providing the atom-scale details of HFBII's hydrophobic patch which in turn provides leads for the engineering of more tightly-coupled interfaces.

Electronic supplementary material The online version of this article (doi:10.1007/s00894-010-0887-1) contains supplementary material, which is available to authorized users.

C. Moldovan · D. Thompson (✉)
Theory Modelling and Design Centre, Tyndall National Institute, University College Cork,
Cork, Ireland
e-mail: damien.thompson@tyndall.ie

Keywords Bio/ICT interfacing · Computer simulation · Hydrophobin · Molecular dynamics · Nanobiotechnology · Protein engineering · Self-assembly · Silicon technology

Introduction

One of the most promising areas of research in nanobiotechnology concerns the technological utilization of self-assembly systems, where molecules spontaneously associate into reproducible supramolecular structures [1]. The importance of such "bottom-up" processes lies in their capability to build uniform, ultra-small functional units and the possibility to exploit such structures at nano-, meso- and macro-scopic scale for both life science and nanotechnology applications [2, 3]. More, the interface between biology, chemistry and material sciences opens a great variety of new opportunities for innovations in nanosciences and biomimetics [4]. In this context, crystalline bacterial cell surface layer (S-layer) proteins [5] of prokaryotic organisms represent a neat self-assembly system which can be exploited as the patterning element for a biomolecular construction kit involving all major species of biological molecules, and have been used as sensing layers for label free detection systems, as matrices for binding immunoglobulins, and in the case of liposomes, as novel targeting and delivery systems.

Another important category of self-assembling proteins are the hydrophobins [6], which show similar properties as the S-layer proteins but are more ordered and consequently of potentially greater utility in Bio/ICT applications. The biophysical properties of the isolated proteins are remarkable, such as strong adhesion, high surface activity and the formation of various self-assembled structures. The protein contains about 100 amino acids, and the surface is mainly hydrophilic, but two β-hairpin

loops contain several sidechains that form a flat "hydrophobic patch" that makes the molecule amphiphilic. They are the most powerful surface-active proteins known and due to the amphiphilic nature and self-assembly properties, applications range from using hydrophobins as surfactants, emulsifiers, and platforms for bionanotechnology applications. The structure and dimensions of the protein molecule are shown in Fig. 1. The existence of the hydrophilic region and hydrophobic patch leads to formation of an ordered protein film, for example, at the air-water interface. Experiments also show [7–10] that it is possible to deposit the hydrophobins selectively on silicon (a hydrophopic surface, as distinct from hydrophilic silicon dioxide) directly from liquid suspension. The formation of the ordered monomolecular film guarantees the ability to control the orientation and reproduce the measurement configuration, typically missing when working with other (bio)molecules. The hydrophobins can also be engineered by attaching other proteins or metal nanoparticles for further functionalization. The present work provides the atom-scale details of the hydrophobic interaction between hydrophobins and silicon in water, complementing the existing Xray [8] and conducting AFM [10] data and providing leads for rational design of interfaces tailored for specific technological applications [9, 11]. The simulations identify the *most* surface-adhesive residues in the hydrophobic patch identified in the Xray structure by the large cluster of uncharged residues comprised of Val18, Leu19, Leu21, Ile22, Val24, Val54, Ala55, Val57, Ala58, Ala61, Leu62 and Leu63.

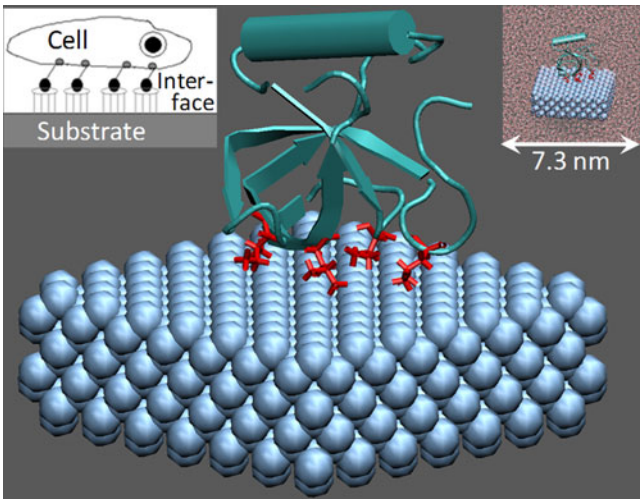

Fig. 1 Representative molecular dynamics structure calculated for the HFBII/Si interface. Structure shows the Si(111) surface as blue van der Waals's spheres and the protein is shown in cartoon representation with hydrophobic patch residues within 0.3 nm of silicon shown as red sticks with waters omitted for clarity; the full solvated cell is shown in the righthand inset. The lefthand inset is a schematic for one possible means of cell attachment to patterned, in this case monolayer-coated, electronics platforms using multivalent linker:monolayer guest:host linkages as drawn

Identification of the protein hydrophobic patch residues driving immobilization provides leads for the synthesis of novel building blocks for future nanoelectronics, exploiting the rather unique properties of hydrophobin proteins that form ordered two-dimensional monolayers on hydrophobic surfaces, such as graphite, graphene and silicon [12]. Furthermore, the proteins show very sharp resonances in current-voltage curves at room temperature [10] and so knowledge of the atom-scale structure, dynamics and energetics is key, since conformal changes in the protein (both in the present native form and in future engineered mutant forms) will affect the current and so dictate the potential of the protein to act as an electromechanical amplifier in, *e.g.*, sensing applications.

To put the hydrophobin:silicon Bio/ICT interface into context, many different biomolecules have been successfully immobilized on Si surfaces, among them modified peptides, saccharides and nucleic acids. For example, DNA molecules have been immobilized on the silicon surface by conjugation to an amine-modified Si surface [13, 14]. A recent combined experimental/simulation study [15] of the interactions of luminescent enzyme luciferase and green fluorescent proteins with silicon substrates found that luciferase adsorbs directly on a hydrophobic Si substrate, and via water molecules on hydrophilic SiO_2. The adsorption induced changes in conformation of luciferase are smaller on the hydrophilic Si substrate than on the hydrophobic one. The more-ordered hydrophobin on the other hand immobilizes directly on silicon using the hydrophobic patch defined from the Xray data [8]. Another material with great potential as a support for biomolecules, and to which hydrophobin proteins bind [12], is graphene, a single-atom-thick sheet of graphite that combines aspects of semiconductors and metals, which can also be "rolled up" into a carbon nanotube. Graphene, like silicon and unlike silicon dioxide, is hydrophobic but has electricity conduction about 100 times greater than that of silicon and could offer many improvements to biochemical sensors [12, 16].

The main aim of the present work was to increase knowledge of how ICT and Bio materials interact and form interfaces. The insights obtained from the computer simulations complement experimental knowledge of the atom-scale adhesion mechanisms by providing new knowledge on the nanoscale structure, dynamics and energetics of protein film assembly on silicon. The knowledge generated will also feed into ongoing efforts to advance directed self-assembly (*e.g.*, dendrimer-linked protein:monolayer assembly), drug design (*e.g.*, identification of biological materials that can adhere to silicon-based delivery systems), and cell immobilization (*e.g.*, for tissue engineering). The societal benefits of advanced bionanotech

devices, all of which require a controllable interface between the Bio and ICT sides, include cheaper, more accurate point-of-care diagnostic devices and more specific, less toxic drugs.

Computational methods

The starting protein structure was generated from a 1.0 Å resolution class II hydrophobin HFBII dimer X-ray structure from the *Trichoderma reesei* fungus [8], PDB code 1R2M. The protein was placed in a cubic cell of edge length 7.3 nm, along with a 2000 atom Si (111) substrate slab and the full protein:silicon model was then solvated with TIP3P water [17] as shown in Fig. 1. For simplicity, Si surface termination was neglected, *i.e.*, Si-H surface groups were not included in the model. The Si substrate model may be thus considered a generic hydrophobic "slab", similar to, *e.g.*, Au(111) or graphene, but with the Si(111) lattice constant of 0.39 nm between hexagonally-packed surface atoms. Si-H termination would give effectively the same surface lattice constant between binding sites with similar steric energies for methyl-carbon$_{HFBII}$:hydrogen$_{Si(111)}$ contacts compared with methyl-hydrogen:silicon contacts and the mutually-compensating balance between short-range H:H repulsion and longer-range C:H and H:Si attraction may be expected to give only mild electrostatic stabilization. Hence, the bare Si(111) surface serves as a useful first approximation to the aqueous Si-H terminated surface and may be expected to generate similar protein interaction structures and dynamics, together with identification of the most surface-active hydrophobic patch residues that drive hydrophobin surface immobilization. Various models were generated, featuring progressively closer protein:silicon starting separations. All structures were minimized with respect to the CHARMM force field [18] supplemented with silicate parameters [19], brought to room temperature and equilibrated for 2 ns with gradually-loosening restraints on the protein backbone heavy atoms, and then subjected to 5 ns of production dynamics. Substrate silicon atoms were constrained to their starting lattice positions throughout the simulations. In all, over 40 ns of dynamics were performed. We employed periodic boundary conditions and a constant volume and temperature ensemble for dynamics, together with a Particle Mesh Ewald treatment of electrostatic interactions. We used the NAMD program [20] for all calculations. Ewald summation was used to calculate the electrostatic interactions and a 2 fs timestep used for dynamics by constraining covalent bonds to hydrogen via the ShakeH algorithm [20]. To the best of our knowledge, to date MD studies of only the class I hydrophobins SC3 and EAS have appeared in the literature, and describe interfacial folding and dynamics [21, 22].

Results

Structure and dynamics of HFBII

Table 1 reports protein stability and flexibility parameters measured over the molecular dynamics runs. Protein root mean square deviations (RMSD) away from the Xray structure [8] and fluctuations (RMSF) around the time-averaged MD structure are modest, with full protein RMSD and RMSF values on the order of 0.10–0.20 and 0.05–0.10 nm respectively. This is accompanied by the expected slightly higher flexibility in the sidechain compared with backbone groups. Hydrophobic patch residues are generally more ordered than the full protein, though the β-barrel composed of disulfide bridges Cys14:Cys26 and Cys53:Cys64 is particularly well ordered with very low RMSD/RMSF values on the order of 0.05 nm, which may be important for tunneling paths through the protein [10].

The radial distribution function RDF plots in Fig. 2 describe some important features of the internal structure of HFBII, namely the two phenylalanine-centered hydrophobic pockets identified in the crystal structure [8]. Image generation and Tcl script-based trajectory analysis for this and all subsequent analyses, was performed using the VMD program [23]. Phe8 neighbors are Leu7, Leu63 and Val54, while Ph39 forms a hydrophobic islet surrounded by nearby hydrophobic residues Pro11, Pro29 Pro50, Ala67, Val2 and Val33. The structures were generated arbitrarily for the model with starting protein:silicon 0.2 nm separation; very similar structures, as reflected in the very similar total RDF plots for each model as given in Supporting Information, were obtained for the other structures generated with more distant protein/silicon starting separations. The RDF plots show generally sharp peaks for close contacts of <0.5 nm with peak widths of 0.1–0.2 nm. Peaks broaden for more distant contacts, reflecting the lower rigidity away from the pockets centers, with peak widths broadening to 0.2–0.4 nm. The generally more dynamics contacts in the larger Phe39 pocket reflect the variety of near-iso-energetic hydrophobic contacts that can form between the seven residues.

Table 1 shows that hydrogen bonds are concentrated largely in the hydrophilic regions away from the hydrophobic patch as expected, with the low H-bond populations in the patch composed of only short-lived weak inter-backbone carboxylate-ammonium contacts that arise sporadically during the MD runs, a typical distribution being Leu21-Val18 (6%), Val18-Ile22 (39%), Ile22-Val18 (11%), Val54-Leu63 (3%) and Leu21-Leu19 (6%). Finally, there is

Table 1 Structure and dynamics of the HFBII protein as it assembles via its hydrophobic patch on Si(111)

Initial protein-surface distance (nm)	Protein stability and flexibility						
	Backbone		Sidechain		β-barrel		H-bonds
	RMSD (nm)	RMSF (nm)	RMSD (nm)	RMSF (nm)	RMSD (nm)	RMSF (nm)	(no. of bonds)
1.2	$0.11_{0.02}$	$0.07_{0.01}$	$0.15_{0.02}$	$0.10_{0.02}$	$0.05_{0.01}$	$0.04_{0.01}$	$12.3_{2.8}$
Patch residues	$0.10_{0.02}$	$0.06_{0.01}$	$0.13_{0.02}$	$0.09_{0.02}$			$0.7_{0.7}$
1.0	$0.13_{0.02}$	$0.07_{0.02}$	$0.17_{0.02}$	$0.11_{0.02}$	$0.06_{0.01}$	$0.04_{0.01}$	$11.7_{2.6}$
Patcxh residues	$0.08_{0.02}$	$0.06_{0.02}$	$0.15_{0.02}$	$0.10_{0.02}$			$0.6_{0.6}$
0.8	$0.14_{0.02}$	$0.09_{0.01}$	$0.22_{0.05}$	$0.14_{0.02}$	$0.05_{0.01}$	$0.04_{0.01}$	$11.5_{2.8}$
Patch residues	$0.08_{0.01}$	$0.06_{0.02}$	$0.16_{0.03}$	$0.10_{0.02}$			$0.6_{0.7}$
0.6	$0.13_{0.03}$	$0.08_{0.02}$	$0.18_{0.04}$	$0.12_{0.02}$	$0.05_{0.01}$	$0.04_{0.01}$	$11.8_{2.8}$
Patch residues	$0.08_{0.01}$	$0.05_{0.01}$	$0.14_{0.02}$	$0.09_{0.02}$			$0.7_{0.7}$
0.4	$0.13_{0.03}$	$0.08_{0.01}$	$0.18_{0.03}$	$0.12_{0.01}$	$0.05_{0.01}$	$0.04_{0.01}$	$12.0_{2.7}$
Patch residues	$0.10_{0.03}$	$0.06_{0.02}$	$0.14_{0.03}$	$0.09_{0.02}$			$0.6_{0.7}$
0.2	$0.16_{0.03}$	$0.08_{0.02}$	$0.20_{0.03}$	$0.12_{0.02}$	$0.05_{0.02}$	$0.04_{0.01}$	$11.3_{2.7}$
Patch residues	$0.13_{0.03}$	$0.07_{0.01}$	$0.18_{0.05}$	$0.12_{0.01}$			$0.5_{0.7}$

The first row for each model gives the total HFBII protein values; the second row gives values for just the hydrophobic patch residues, *i.e.*, Val18, Leu19, Leu21, Ile22, Val24, Val54, Ala55, Val57, Ala58, Ala61, Leu62 and Leu63. Root mean square deviations and fluctuations RMSD and RMSF are computed from 5 ns (2000 structures) of room temperature molecular dynamics for each model. MD structures were first of all aligned to filter out protein centre of mass motions. Time-averaged standard deviations are given as subscripts

generally little dependence of protein stability and flexibility on the starting protein:silicon separation. The most noticeable effect is the shift to slightly higher patch sidechain RMSD/RMSF values that approach 0.20/0.15 for the interface-forming models, *i.e.*, those with starting separations of 0.8, 0.4 and 0.2 nm as described in the next section. These shifts are due to patch ordering on silicon with the relatively large time-averaged standard deviations reflecting the dynamic interfaces formed as described in the next section that retain some mobility in the patch residues as they cycle between flat inter-patch stabilizing conformations and more protruding patch-surface stabilizing conformations.

Immobilization on Si(111) via hydrophobic patch binding

Figure 3 shows how an energetically-favorable interface forms between the HFBII hydrophobin protein and bare Si (111). The hydrophobic patch residues contribute 70–80% of the overall protein binding energy. The noise in the binding energy plots reflects the weakness and only moderate directionality of the hydrophobic van der Waals's interface formed between the patch and silicon. Interestingly, the starting 0.8 nm separation structure finds a stable interface while the initially closer 0.6 nm starting separation structure remains in solution, illustrating the rather flat potential energy surface for the weak protein:silicon interaction and the need for multiple, multi-nanosecond simulations. Si surface terminations of Si-H and/or Si-OH in aqueous solution, not incorporated into the present models, may provide relatively stronger, more site-specific and hence longer-lived local interactions, and will be addressed in future work as hybrid ICT/Bio force fields continue to evolve [24].

Three models, those with starting separations of 0.8, 0.4 and 0.2 nm, form similar stable interfaces, with the hydrophobic patch tilted to maximize silicon-mediated desolvation of aliphatic residues while allowing also solvation of charged residue Asp59. HFBII in the starting 0.2 nm separation structure pushes away from the surface due to steric repulsion of the too-close initial interface contacts and then rebinds in a better orientation with Asp59 tilted up and in a more favorable solvated environment. The 0.8 and 0.4 nm starting separation structures show similar dynamics, quickly finding a rather flat patch:silicon interface which subsequently tilts upwards on the side of the Asp59 residue to simultaneously maximize hydrophobic and hydrophilic interactions.

The Asp59 sidechain remains solvated and so unbound to Si(111), driving tilting of the patch. As such, Asp59 serves as a prime candidate for engineering via site-directed mutagenesis. MD structures show Asp59 exposed to solvent and coordinated to both (continuously exchanged bulk) waters and also nearby Gln60, Ala61 backbone ammonium groups. Hence, Asp59 mutation may affect the overall conformational stability of the patch. Another possible disadvantageous effect of Asp59 mutation may be due to its role in channeling water molecules away from

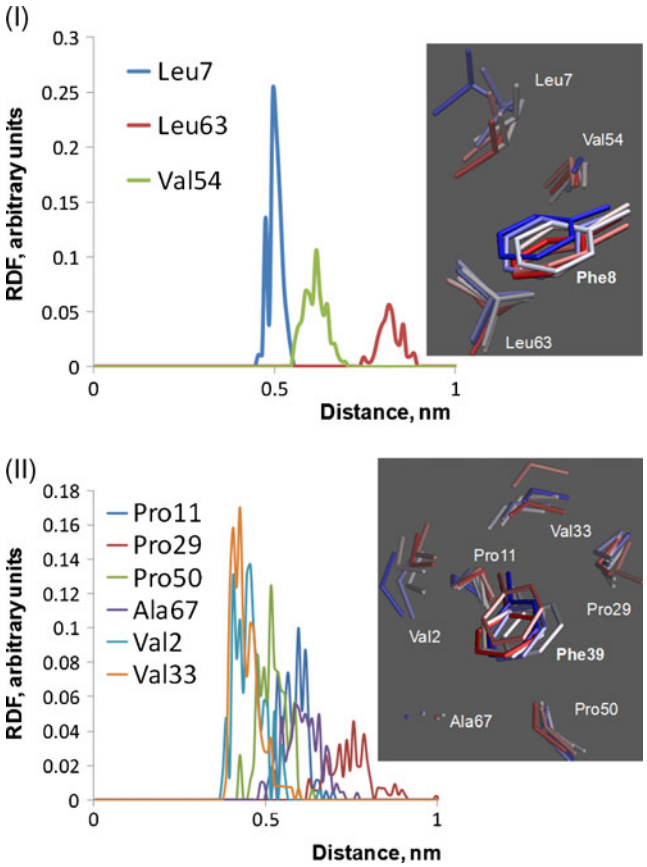

Fig. 2 Radial distribution functions RDF for the phenylalanine-centered hydrophobic pockets (I) Phe8 and (II) Phe39, showing inter-Cβ contacts to neighbouring residues identified from the crystal structure [8]. Righthand panels show pocket sidechains, with representative structures colored from red to white to blue over the 5 ns of equilibrated dynamics

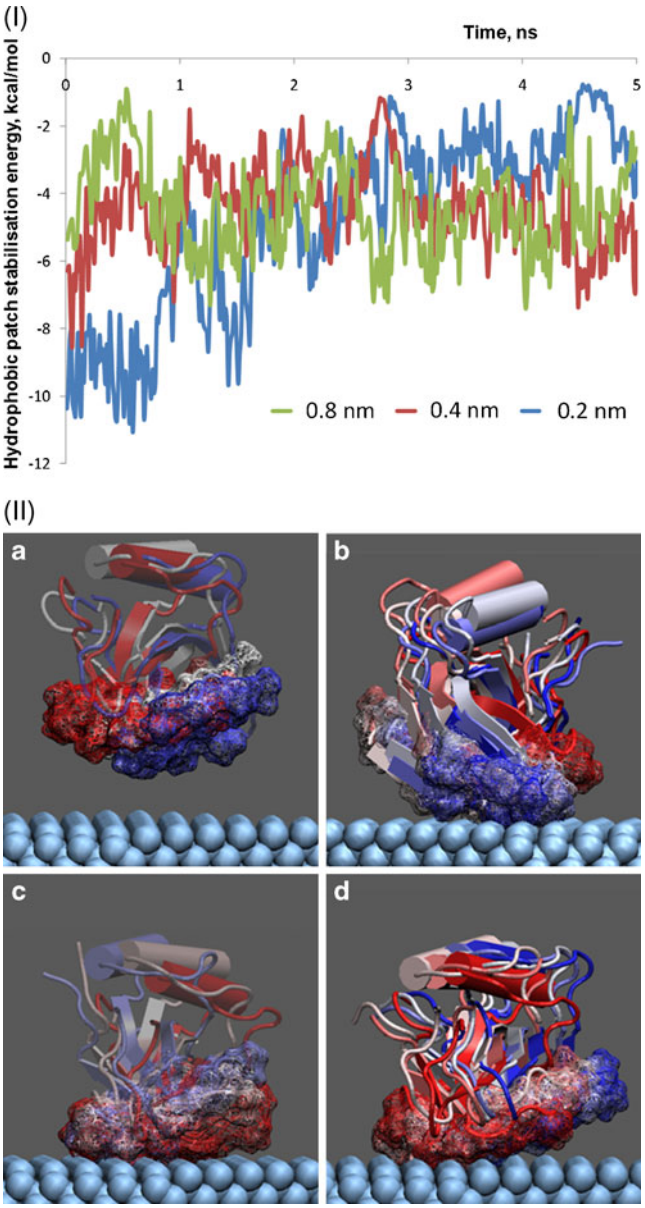

Fig. 3 Energy profile and dynamics for HFBII adsorption on the Si (111) surface. Panel (I) shows interaction energies between the hydrophobic patch and Si(111) for the structures that formed van der Waals's interfaces, those with starting separations of 0.8, 0.4 and 0.2 nm. Panel (II) shows molecular dynamics structures for the HFBII/Si(111) interface generated from starting structures with HFBII initially (**a**) 1.2 (reference unbound structure), (**b**) 0.8, (**c**) 0.4 and (**d**) 0.2 nm above the silicon surface. Structures show the Si(111) surface as blue van der Waals's spheres and the protein is shown in cartoon representation with the hydrophobic patch residues shown as wireframe van der Waal's surfaces. Protein structures are superimposed in each panel, with structures colored from red to white to blue over the 5 ns of equilibrated dynamics, and waters omitted for clarity

patch residues Ala61 and Leu63, the only residues that show significantly lowered solvation energies upon interface formation (Fig. 3, where solvation energies are given as the time-averaged residue:water interaction energies) with Leu63 also the strongest silicon binder (Fig. 3). These competing hydrophobic push and hydrophilic pull drivers in interface coupling/decoupling illustrate the nanoscale effects that are difficult to decipher from experiments alone and which need to be considered for rational engineering.

Figure 4 highlights the patch residues contributing most strongly to surface immobilization. Per-residue contributions to the hydrophobic patch:Si(111) interaction energies are given in Supporting Information, along with a movie (interface.gif) showing the MD structures sampled for the interface with starting separation of 0.2 nm. In solution, protein patch residues in the more open regions (Fig. 4a(I)) have stronger coordination of water molecules. In particular, near-Asp59 residues, alanines Ala61 and Ala58 show large solvation energies. Ala61 makes a (relatively small) contribution to patch immobilization in two of the three formed interfaces (Fig. 4b, c) and shows significant desolvation upon binding to silicon, its solvation energy reduced from −19±4 to −12±4 kcal mol^{-1}. The remaining patch residues driving immobilization are at the side of the patch furthest from Asp59, with leucines

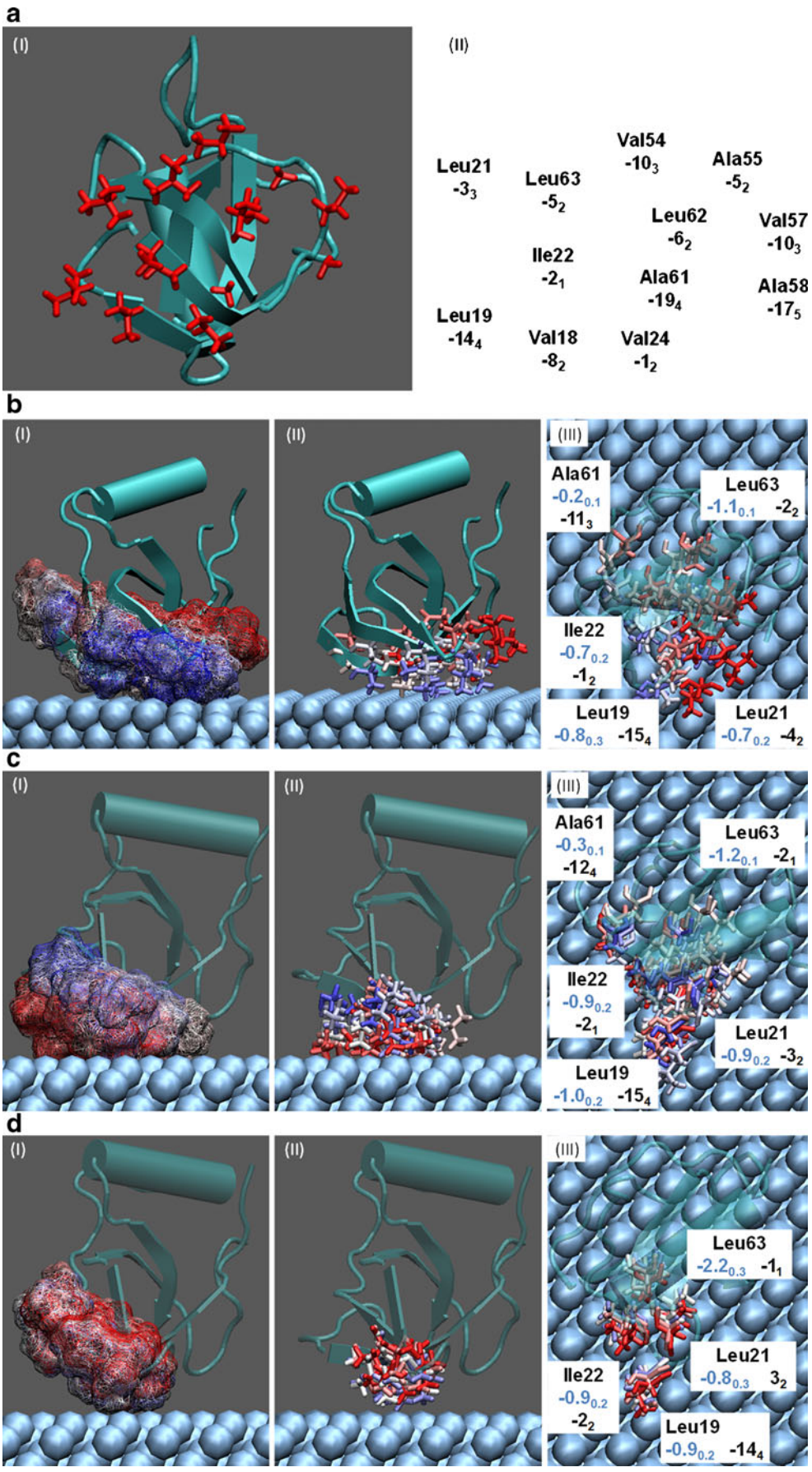

Fig. 4 Structure and dynamics of the HFBII/Si(111) interface, from the (**a**) reference unbound structures and (**b**) 0.8, (**c**) 0.4 and (**d**) 0.2 nm starting separation models that form interfaces. Panel (**a**) shows the patch residues as red sticks in the reference unbound structure (I) together with per-residue solvation energies (II) for hydrophobic patch residues averaged over the 6000 unbound structures produced from 5 ns each for models with starting separations of 1.2, 1.0 and 0.6 nm. Three subpanels are then given for each interface model (**b**), (**c**) and (**d**). Lefthand panels (I) show the full hydrophobic patch as van der Waals's spheres and structures colored from red to white to blue over the 5 ns of equilibrated dynamics. Middle panels (II) highlight the most adhesive hydrophobic patch residues Leu19, Leu21, Ile22, Leu63 and in some cases Ala61. Righthand panels (III) show corresponding plan views of the interface. Residue components to the silicon adsorption (blue) and solvation energies (black) are averaged over the final 2 ns ns of dynamics for each model, using ~500 bound structures calculated for each of the interface models (**b**), (**c**) and (**d**). Residue-based binding energy timelines are given in Supporting information

Leu19, Leu21 and particularly Leu63, along with isoleucine Ile22, exhibiting significant silicon binding energies of ~−1 to −2 kcal mol^{-1} and in the case of the strongest-binder Leu63, also significantly reduced solvation from −5±2 to −2±2 kcal mol^{-1}.

Figure 5 shows a representative tightly-bound interface, the final MD structure for the model with starting separation of 0.2 nm. From left to right, Leu19, Leu21, Ile22, Ala61 and Leu63 sidechains all make close van der Waals's contacts to silicon; the full 5 ns of dynamics are given in the movie interface.gif in Supporting Information. The methyl groups form optimum van der Waals's contacts to silicon as shown in the bottom panel of Fig. 5. The binding to monatomic Si(111) is in some features reminiscent of alkanethiol self-assembled monolayer (SAM) formation on Au(111) which, though featuring stronger electrostatic thiol:Au interactions, is in the early stages of assembly prior to thiol:Au covalent bonding, also poorly directional [25]. Similarly for hydrophobin immobilization,

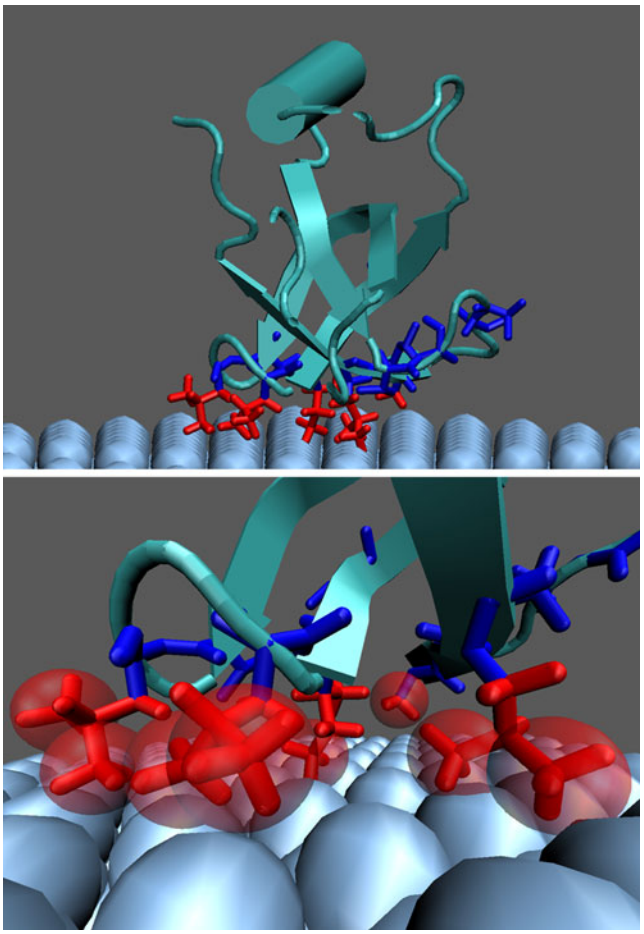

Fig. 5 Representative tightly-bound HFBII/Si(111) interface. The full hydrophobic patch is colored blue with the most adhesive residues colored red. The bottom panel gives a zoomed-in perspective view with the near-silicon methyl carbons shown as transparent van der Waals's spheres

the weakness of the individual patch residue-silicon interactions providing for a flexible, self-correcting interface which, over time and due to the overall moderate binding energy summed over all the binding residues (Fig. 3), results in formation of an ordered film on the substrate.

Discussion

Self-assembly and molecular recognition are used extensively by nature to build complex structures via specific non-covalent guest:host interactions. Understanding recognition mechanisms in physical and chemical terms means accessing the information contained in (macro)molecules, crucial for understanding interactions such as antigen:antibody and ligand:enzyme recognition, and the design of new molecules with tailored recognition properties. In recent years, synthetic materials like "molecular printboards" [26] and biological materials like hydrophobin proteins [10] have been used to marry the power of (bio)molecular recognition with existing materials for electronics including silicon, gold, silica and graphene [12, 26]. This combination provides novel hybrid Bio/ICT materials that can recognize specific molecules and so control the adhesion and transport of material at, and through, interfaces including for example nanoparticle "printing" on solvated gold-bound monolayers [26], protein film growth on silicon [12] and DNA sensing at aqueous/organic liquid-liquid interfaces [27]. Just one illustrative promising application that combines the new knowledge generated in these fields is the tethering of macromolecules to silicon to provide a means of cell immobilization for Bio/ICT applications including electronically-responsive tissue engineering [28], as sketched in Fig. 1. Native and re-engineered HFBII proteins may provide a more ordered alternative interface for direct attachment, without the need for substrate patterning. In the drawing in Fig. 1, the interface can be composed of a substrate-bound monolayer functionalized with receptor molecules (*e.g.*, calixarene, cyclodextrin hosts), that recognize the cell surface, either directly via peptides that bind to the host pockets or via, *e.g.*, linear or dendritic linkers that are functionalized, as drawn, at either end for host and cell recognition [26]. Commonly used electronics substrate materials include silicon, silica, transparent metal oxide films, graphene and carbon nanotubes [12].

Interfaces thus add phase separation and transport to the already-potent mix of self-assembly and molecular recognition in single phases. This power brings with it myriad potential applications but also enormous challenges in understanding molecular behavior in multi-phases and interface adhesion/penetration, some of which are addressed in the current work. The new knowledge generated on the mecha-

nism of protein adhesion on silicon will provide leads for the development and optimization of interfacial phenomena in existing and emerging applications such as sensing and ion transport [27], drug delivery [29, 30] and Bio/ICT interfacing [31, 32]. The development of novel hybrid Bio/ICT functional interfaces is an exploding field [31, 32]—the development of platforms for electronically-responsive tissue engineering is just one illustrative example. Molecular simulation can provide crucial high-level mechanistic detail to complement and guide experimental efforts to understand and rationally modify synthetic nanomaterials, biomaterials and hybrid nano/bio systems [33–39].

Conclusions

Interfaces are the gate keepers that regulate the molecular interactions fueling living systems and are now also becoming ubiquitous in nanotechnology and bionanotechnology where binding at interfaces, and in some cases transport through interfaces, allows for the self-assembly of highly-ordered functional "nanomachines" which may or may not incorporate some bio components. Experimental testing remains the primary way of measuring key properties and behavior but cannot test everything; understanding the mechanisms requires detailed nanoscale experiments and simulations and so the focus of the present work is on complementing and deepening experimental knowledge of atom-level detail using computer simulations. Complex architectures can self-assemble at the nanoscale using molecular "gluing", reversible non-covalent interactions that act collectively to give tightly-woven self-correcting and self-healing assemblies; molecular simulations may be used to compute the structure, dynamics and energetics of self-assembly, uncovering the atom-scale mechanisms and providing leads for experiment in the design of more complex, more heterogeneous materials.

The atom-scale details of the protein/silicon interface obtained in the present study will aid experimental efforts to better understand the role of interfaces in materials adhesion, both in itself and as a first step in subsequent separation and transport events. Specifically, the potential to combine the proteins in a controlled manner with silicon nanoelectronics opens new possibilities for integrated bionanoelectronics. The simulations reveal the interactions that underlie and drive the creation of the stable immobilized structure through which the conducting paths through the proteins can interface with silicon. In particular, a subset of hydrophobin residues, namely three leucines, one isoleucine and one alanine, were identified as the main contributors to immobilization, with a charged aspartate opposing binding and possibly providing a target for site-directed mutagenesis engineering of more adhesive hydrophobin structures. Modeling thus forms a crucial part of understanding the mechanisms, complementing the earlier optical and electrical characterization [7–10]. In closing, the atom-scale structure of the interface provides new fundamental science and crucial data for the design and optimization of integrated Bio/ICT applications including sensing, materials transport, drug design and potentially most useful of all, nanopatterning of silicon substrates with biological macromolecules for applications such as scaffold-mediated cell immobilization for electronically-responsive tissue engineering.

Acknowledgments We wish to acknowledge support for this research from Science Foundation Ireland (SFI) under the UREKA Programme and also Enterprise Ireland Innovation Partnership project ORD3D. We acknowledge SFI for computing resources at Tyndall National Institute and SFI/ Higher Education Authority for computing time at the Irish Centre for High-End Computing (ICHEC).

References

1. Aggeli A, Bell M, Boden N, Keen JN, Knowles PF, McLeish TC, Pitkeathly M, Radford SE (1997) Nature 386:259–262
2. Colombo G, Soto P, Gazit E (2007) Trends Biotechnol 25:211–218
3. Whitesides GM, Lipomi DJ (2009) Faraday Discuss 143:373–384
4. Nosonovsky M, Bhushan B (2008) Adv Func Mater 18:843–855
5. Pum D, Neubauer A, Györvary E, Sára M, Sleytr UB (2000) Nanotechnol 11:100–107
6. Talbot NJ (1999) Nature 398:295–296
7. Wösten HA, van Wetter MA, Lugones LG, van der Mei HC, Busscher HJ, Wessels JG (1999) Curr Biol 9:85–88
8. Hakanpaa J, Paananen A, Askolin S, Nakari-Setala T, Parkkinen T, Penttila M, Linder MB, Rouvinen J (2004) J Biol Chem 279:534–539
9. Szilvay GR, Paananen A, Laurikainen K, Vuorimaa E, Lemmetyinen H, Peltonen J, Linder MB (2007) Biochemistry 46:2345–2354
10. Kivioja JM, Kurppa K, Kainlauri M, Linder MB, Ahopelto J (2009) Appl Phys Lett 94:183901
11. Zhao ZX, Qiao MQ, Yin F, Shao B, Wu BY, Wang YY, Wang XS, Qin X, Li S, Yu L, Chen Q (2007) Biosens Bioelectron 22:3021–3027
12. Laaksonen P, Kainlauri M, Laaksonen T, Shchepetov A, Jiang H, Ahopelto J, Linder M (2010) Angew Chem Int Ed 49:4946–4949
13. Lin Z, Strother T, Cai W, Cao X, Smith LM, Hamers RJ (2002) Langmuir 18:788–796
14. Streifer JA, Kim H, Nichols BM, Hamers RJ (2005) Nanotechnology 16:1868–1873
15. Nishiyama K, Hoshino T (2007) Appl Phys Lett 90:213901
16. Ziegler KJ (2005) Trends Biotechnol 23:440–428
17. Jorgensen W, Chandrasekhar J, Madura J, Impey R, Klein M (1983) J Chem Phys 79:926–935
18. MacKerell AD, Bashford D, Bellott M, Dunbrack RL, Evanseck JD, Field MJ, Fischer S, Gao J, Guo H, Ha S et al (1998) J Phys Chem B 102:3586–3616
19. Lopes PEM, Murashov V, Tazi M, Demchuk E, MacKerell AD Jr (2006) J Phys Chem B 110:2782–2792
20. Phillips JC, Braun R, Wang W, Gumbart J, Tajkhorshid E, Villa E, Chipot C, Skeel RD, Kale L, Schulten K (2005) J Comput Chem 26:1781–1802
21. Fan H, Wang X, Zhu J, Robillard GT, Mark AE (2006) Proteins 64:863–873

22. Kwan AH, Macindoe I, Vukasin PV, Morris VK, Kass I, Gupte R, Mark AE, Templeton MD, Mackay JP, Sunde M (2008) J Mol Biol 382:708–720
23. Humphrey W, Dalke A, Schulten K (1996) J Mol Graph 14:33–38
24. Iori F, Di Felice R, Molinari E, Corni S (2009) J Comput Chem 30:1465–1476
25. Love JC, Estroff LA, Kriebel JK, Nuzzo RG, Whitesides GM (2005) Chem Rev 105:1103–1170
26. Huskens J (2006) Curr Opin Chem Bio 10:537–543
27. Kivlehan F, Lefoix M, Moynihan HA, Thompson D, Ogurtsov VI, Herzog G, Arrigan DWM (2010) Electrochim Acta 55:3348–3354
28. Chan G, Mooney DJ (2008) Trends Biotechnol 26:382–392
29. Hearn EM, Patel DK, van der Berg B (2008) Proc Natl Acad Sci USA 105:8601–8606
30. Valo HK, Laaksonen PH, Peltonen LJ, Linder MB, Hirvonen JT, Laaksonen TJ (2010) ACS Nano 4:1750–1758
31. Zheng G, Patolsky F, Cui Y, Wang WU, Lieber CM (2005) Nature Biotechnol 23:1294–1301
32. Hiratsuka Y, Miyata M, Tada T, Uyeda TQP (2006) Proc Natl Acad Sci USA 103:13618–13623
33. Carter EA (2008) Science 321:800–803
34. Klein MK, Shinoda W (2008) Science 321:798–800
35. Ander M, Luzhkov VB, Aqvist J (2008) Biophys J 94:820–831
36. Meinhold L, Smith JC, Kitao A, Zewail AH (2007) Proc Nat Acad Sci 104:17261–17265
37. Thompson D (2007) Langmuir 23:8441–8451
38. Thompson D, Miller C, McCarthy FO (2008) Biochemistry 47:10333–10344
39. Gannon G, Greer JC, Larsson JA, Thompson D (2010) ACS Nano 4:921–932